Electronic and thermoelectric properties of RuIn$_{3-x}$A$_x$ (A = Sn, Zn)

Deepa Kasinathan,[1] Maik Wagner,[1] Klaus Koepernik,[2] Raul Cardoso-Gil,[1] Yu. Grin,[1] and Helge Rosner[1]

[1]*Max-Planck-Institut für Chemische Physik fester Stoffe, D-01187 Dresden, Germany*
[2]*IFW Dresden, P.O. Box 270116, D-01171 Dresden, Germany*

Recently, we reported [M. Wagner *et al.*, J. Mater. Res. **26**, 1886 (2011)] transport measurements on the semiconducting intermetallic system RuIn$_3$ and its substitution derivatives RuIn$_{3-x}$A$_x$ (A = Sn, Zn). Higher values of the thermoelectric figure of merit ($zT = 0.45$) compared to the parent compound were achieved by chemical substitution. Here, using density functional theory based calculations, we report on the microscopic picture behind the measured phenomenon. We show in detail that the electronic structure of the substitution variants of the intermetallic system RuIn$_{3-x}$A$_x$ (A = Sn, Zn) changes in a rigid-band-like fashion. This behavior makes possible the fine tuning of the substitution concentration to take advantage of the sharp peaklike features in the density of states of the semiconducting parent compound. Trends in the transport properties calculated using the semiclassical Boltzmann transport equations within the constant scattering time approximation are in good agreement with the former experimental results for RuIn$_{3-x}$Sn$_x$. Based on the calculated thermopower for the *p*-doped systems, we reinvestigated the Zn-substituted derivative and obtained ZnO-free RuIn$_{3-x}$Zn$_x$. The new experimental results are consistent with the calculated trend in thermopower and yield a large zT value of 0.8.

I. INTRODUCTION

Thermoelectric materials, capable of creating electricity from waste heat, are ideal in the search for sustainable energy resources. The bulk of present day efficient thermoelectric materials have one common feature: all are heavily doped narrow band gap semiconductors with a carrier concentration of 10^{19} to 10^{21} cm^{-3}. In particular, narrow band gap materials with complex crystal structure have been shown to possess excellent thermoelectric properties.[1,2] In general, the efficiency of a thermoelectric material is measured by a dimensionless parameter called the figure of merit, $zT = S^2 \sigma T/(\kappa_{el} + \kappa_{ph})$, where S is the thermopower (Seebeck coefficient) of the material, T is temperature, σ is the electrical conductivity, κ_{el} is the electronic part of the thermal conductivity, and κ_{ph} is the lattice (phonon) contribution to the thermal conductivity. A zT value larger than 1 is imperative for successful applications. Since all the material-related parameters that determine zT are interlinked, tuning each parameter quasi-independently without adversely affecting the other is a tricky endeavor.

Many of the binary compounds formed by transition-metal atoms with groups III, IV, and V elements have been shown to possess electronic band gaps. For example, FeSi, FeSb$_2$, and FeGa$_3$ are all semiconducting with energy gaps of about 0.06, 0.04, and 0.45 eV, respectively.[3–5] The hybridization of the narrow d bands of the transition metals with the rather broad p bands of the p elements has been suggested to assist the formation of such band gaps.[6] In particular, such hybridization also produces sharp features close to the Fermi level, which in turn has been shown to be quite beneficial for enhanced thermoelectric properties.[2,7] Consequently, large thermopower values of $+500$ μV/K at 50 K in FeSi,[8] -45 mV/K at 10 K in FeSb$_2$,[4] and -350 μV/K at 300 K in FeGa$_3$[9] have been evidenced. The compound RuIn$_3$ is isotypic to FeGa$_3$ and was first reported[10] in 1959 and later confirmed by Holleck and co-workers[11] in 1964. Early resistivity measurements reported poor metallic conductivity

in this system,[12] but later, density functional theory based calculations predicted semiconducting behavior.[13] Subsequent measurements have confirmed the semiconducting nature of RuIn$_3$.[13,14] Studies on the thermoelectric properties of RuIn$_3$ do not exist. Recently, we reported the results of the transport measurements of both RuIn$_3$ and its substitution variants RuIn$_{3-x}$A$_x$ (A = Sn, Zn).[15] The substitution variants exhibit relatively large Seebeck coefficients in a wide temperature range along with reduced thermal conductivity compared to the parent semiconductor RuIn$_3$, thereby incorporating them in the family of potential thermoelectric materials. Transport measurements on the binary RuIn$_3$ show semiconducting behavior with a band gap of $\approx$0.45 eV for polycrystalline samples.[15] The binary compound shows multiband features exhibiting a large negative thermopower $S = -363$ μV/K at 308 K and a positive thermopower $S = +262$ μV/K at 461 K.[15] This crossover behavior (electron transport at 308 K to hole transport at 461 K) is suppressed by chemical substitution. The Sn-substituted samples show *n*-type behavior, while the Zn-substituted samples show *p*-type behavior, with a transition from semiconducting to metallic behavior with increasing x. Chemical substitution reduces the thermal conductivity to 50% of the value of the binary compound, resulting in a zT of 0.45 at 630 K for RuIn$_{2.95}$Zn$_{0.05}$, an improvement by a factor of 7 over pure binary phase. The wide chemical versatility of this material, combined with the observance of good thermoelectric properties, suggests that further investigations are necessary to optimize and tune this material and identify similar versatile members (abundant and low-cost alternatives) as viable candidates for future high-temperature thermoelectric applications.

Here, first we present our results on the electronic and transport properties of RuIn$_3$ and the substitution variants using density functional theory (DFT) based calculations to provide a microscopic insight into the physics behind the measured phenomenon. The three theoretical reports on the parent

compound that exist in the literature have mainly focused on evaluating the band structure to obtain an estimate for the band gap.[14,16,17] In the present work, we focus on investigating the changes to the electronic structure as a function of substitution, as well as to probe the dependence of thermoelectric transport properties on the carrier concentration based on first-principles calculations. By doping a semiconductor, one creates a slightly different material, and the changes induced by doping manifest themselves as a transformation of the band structure and, correspondingly, the electronic density of states. Various physical mechanisms, including electron-electron interaction, impurity-band widening, band tailing, and screening effects between the dopant and the host structure play a role in the altering of the band structure.[18] Additionally, the dopant can either be randomly distributed or enter the host structure in an ordered fashion. These varied scenarios can have a profound effect on the electronic structure of the substituted variants, and the resulting band structure could either be a simple rigid-band shift of the semiconducting host compound to account for the additional holes/electrons or a complex scenario with unequal band shifts of the intrinsic band edges. Tuning thermoelectric properties of the parent semiconductor by doping requires a well controlled change in the density of states of the doped variants, thereby accessing the sharp peaklike features close to the Fermi level of the host material. Consequently, it necessitates a careful study of the electronic structure of both the doped and undoped compounds first and the subsequent calculation of the transport properties. In our work, we follow this two-step approach for $RuIn_{3-x}A_x$ (A = Sn, Zn).

In our previous work, we observed small amounts of a ZnO impurity phase and nonreacted elemental Ru in the $RuIn_{3-x}Zn_x$ samples.[15] The presence of these impurity phases may result in the somewhat nonuniform behavior of the resistivity and thermopower values (as a function of x) for $RuIn_{3-x}Zn_x$ in the temperature range $300 \leqslant T \leqslant 600$ K. On the contrary, the thermopower of the Sn-substituted samples decreased uniformly with increasing x. Based on our calculations of the transport properties of these materials (Sec. V), we infer that the thermopower of both n- and p-doped systems should show a uniform behavior. Consequently, we have successfully prepared a new batch of ZnO free $RuIn_{3-x}Zn_x$ ($x = 0.025, 0.050,$ and 0.100) by applying starting materials of higher purity and measured their transport properties.

II. CRYSTAL STRUCTURE

Subsequent to the initial refinement of the crystal structure of $RuIn_3$ within the space group $P\bar{4}n2$ (CoGa$_3$ type), it has been shown that the this compound crystallizes in the higher symmetry of the tetragonal space group $P4_2/mnm$ (No. 136) and belongs to the FeGa$_3$ type of structure.[12] The lattice parameters used in our calculations are $a = 6.999$ and $c = 7.246$Å.[15] The unit cell of $RuIn_3$ contains four formula units, with two crystallographically inequivalent In sites, In1 and In2 (Ru: [0.3451, 0.3451, 0]; In1: [0, 0.5, 0]; In2: [0.1555, 0.1555, 0.2622]).[12] The structure of $RuIn_3$ can be visualized using two basic building blocks in a complementary fashion: (i) each In1 atom sits in the center of a distorted cube formed by eight In2 atoms (Fig. 1, top panel); (ii) around each Ru atom six neighboring In2 atoms form a distorted trigonal prism,
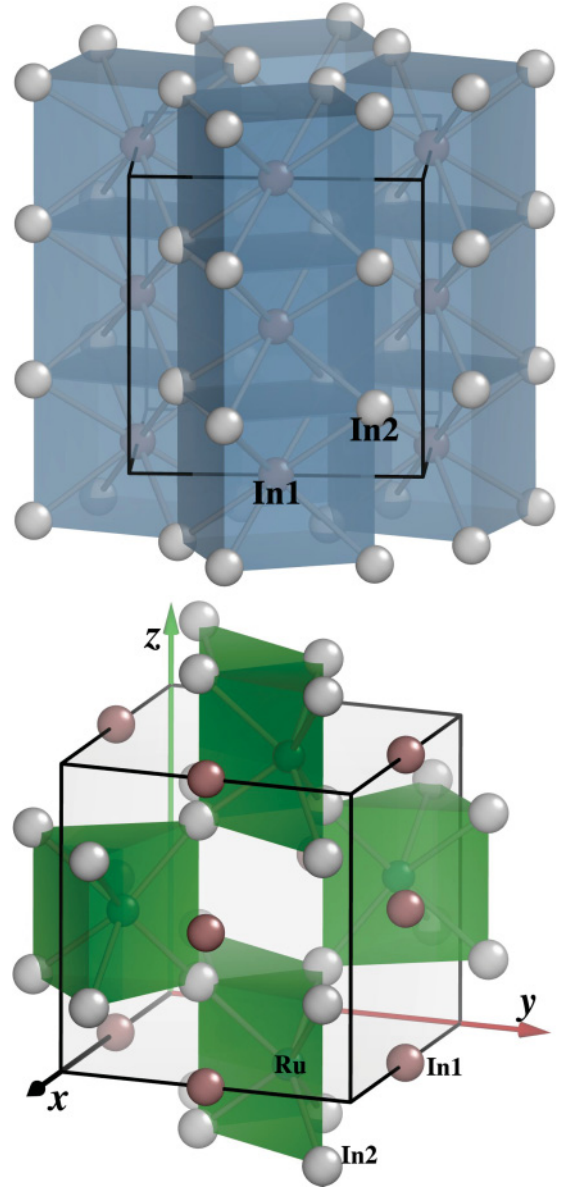

FIG. 1. (Color online) Crystal structure of $RuIn_3$. Top panel shows the distorted cubes formed by In2 atoms, with In1 atoms sitting in the centers. Bottom panel shows the distorted trigonal prisms formed by In2 atoms with Ru atoms at their centers. Two neighboring trigonal prisms share a rectangular face. The prisms and the cubes are interlinked along the c axis by the corner In2 atoms.

with two trigonal prisms sharing a common face. Additionally, the trigonal prisms are interlinked along the crystallographic z direction by sharing In2 corners (Fig. 1, bottom panel). Both building blocks share side faces and form a complex three-dimensional packing of polyhedra, rather than a layered one.

III. CALCULATIONAL DETAILS

Non-spin-polarized DFT total energy and Kohn-Sham band-structure calculations were performed applying the full-potential local-orbital code (version FPLO9.01.35), within the local density approximation (LDA).[19,20] The Perdew and Wang

flavor[21] of the exchange correlation potential was chosen for the scalar relativistic calculations.[22] The calculations were carefully converged with respect to the number of k points, and finally a $24 \times 24 \times 24$ regular k-point mesh [1183] points in the irreducible Brillouin zone (BZ)] was used in the full BZ. The lattice parameters for undoped $RuIn_3$, as well as the doped variants,[23] are taken from Ref. 15. It is well known that the LDA tends to overbind, resulting in lattice constants that are too small. Therefore, the calculations were carried out with experimental lattice constants, while the internal coordinates are relaxed for all the structures considered in this work. The substitutional derivatives $RuIn_{3-x}Sn_x$ and $RuIn_{3-x}Zn_x$ were modeled using three kinds of approaches: the simpler virtual crystal approximation (VCA), the fully disordered coherent potential approximation (CPA, calculated using FPLO5.00),[24] and the ordered supercell (SC) approach. Within the VCA, a virtual atom with the desired number of electrons and protons is substituted at the indium wyckoff positions. We employed the VCA in the following way: the input of our full potential method is the nuclear positions and charges and the basis functions (local orbitals). A virtual atom is constructed such that the number of effective valence electrons equals the one in the disordered alloy approximated by the VCA. This is achieved by choosing an appropriate noninteger nuclear charge and a corresponding equal number of electrons for the disordered sites. The full potential scheme then solves the DFT equations for this unit cell with noninteger nuclear/electron charges, automatically adapting the basis functions and the potential to this nuclear configuration as it does for any other arrangement of "natural" atoms. This choice of VCA reproduces the correct electron filling and often gives very satisfactory results compared to supercell and/or CPA calculations.[25,26] In the CPA, the disorder of the dopant is taken into account explicitly and hence is more reliable, but also more time consuming. Within the CPA, the dopant atom retains its identity, but produces an effective medium that accounts for random disorder, resulting in the incoherence of the bands or more precisely, the spectral function $A(k,\omega)$. The incoherence arises because of the quantum mechanical averaging of the wave functions over the atomic potentials. In the SC approach, one of the indium positions is occupied by the substituent Zn or Sn. Such a construction results in ordering of the substituent, but allows one to quantify specific effects that arise because of the periodicity that is imposed. Two supercells were constructed. The first was constructed by substitution of one In by Zn(Sn) within the tetragonal $P4_2/mnm$ structure unit cell of $RuIn_3$. Since one unit cell contains four formula units, this corresponds to an 8.33% Zn(Sn) substitution and has no Zn-Zn(Sn-Sn) nearest-neighbor pairs. The second cell is a doubled cell along the c axis with eight formula units per unit cell. Again, one In was replaced by Zn(Sn), corresponding to a 4.2% Zn(Sn) substitution. Like the smaller supercell, this cell also has no nearest-neighbor Zn-Zn(Sn-Sn) bonds.

The transport properties were calculated using the semiclassical Boltzmann transport theory[27–29] within the constant scattering approximation as implemented in BOLTZTRAP.[30] This approximation is based on the assumption that the scattering time τ determining the electrical conductivity does not vary strongly with energy on the scale of kT. Additionally,

no further assumptions are made on the dependence of τ due to strong doping and temperature. This method has been successfully applied to many narrow band gap materials including clathrates and as well as to oxides.[29,31–33]

IV. ELECTRONIC STRUCTURE

A. $RuIn_3$

Collected in Fig. 2 are the LDA non-spin-polarized band structure and density of states (DOS) of the tetragonal $RuIn_3$. In the energy range displayed (-3.5 to 2 eV), there is a strong hybridization between the In $5p$ states and the Ru $4d$ states. We obtain a band gap value of 0.3 eV, consistent with previously published results.[14,16,17] It is well known that the Kohn-Sham bands obtained from contemporary exchange correlation approximations underestimate the size of the semiconducting band gaps; hence the calculated band gap of 0.3 eV is naturally slightly smaller than the experimentally observed value of 0.45 eV.[14] From the band structure, we witness that $RuIn_3$ has an indirect band gap with the top of the valence band occurring close to the A point along the $R \Longrightarrow A$ symmetry line, and the bottom of the conduction band is close to the Z point along the $\Gamma \Longrightarrow Z$ line. It is worthwhile to note that the curvature of these two bands are similarly parabolic, resulting in similar values for the effective masses for the holes and electrons at low substitution concentrations. Our results concerning the bottom of the conduction band are consistent with the reports of Imai and co-workers[16] and with that of Mani and co-workers.[17] On the contrary, calculations by Bogdanov *et al.*[14] using the TB-LMTO-ASA (tight binding-linearized muffin tin orbital-atomic sphere approximation) package find the rather flat band along $M \Longrightarrow \Gamma$ as the minimum of the conduction band, thereby yielding a larger effective mass of the holes as compared to electrons. Additionally, the bands are similarly dispersive along the various high symmetry directions, consistent with the three-dimensional nature of
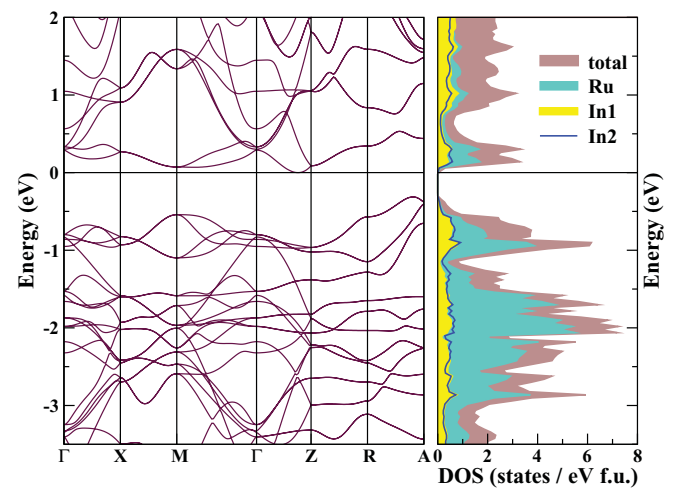

FIG. 2. (Color online) (Left panel) Band structure and (Right panel) total and site projected electronic density of states of non-spin-polarized $RuIn_3$. The band structure is plotted along the standard high-symmetry directions [in units of $(\pi/a, \pi/b, \pi/c)$] of a tetragonal lattice: $\Gamma(0,0,0) \Longrightarrow X(0,1/2,0) \Longrightarrow M(1/2,1/2,0) \Longrightarrow \Gamma \Longrightarrow Z(0,0,1/2) \Longrightarrow R(0,1/2,1/2) \Longrightarrow A(1/2,1/2,1/2)$.

the building blocks in the crystal structure. Our calculations are well in agreement with the recent experimental results on RuIn$_3$.[15]

B. RuIn$_{3-x}$Sn$_x$: electron doping

The consequences of substituting Sn (group IV) for In predicted by the three calculational approaches are displayed in Fig. 3. The top panel compares the total DOS for the various approaches for the 4.2% substitution scenario RuIn$_{2.875}$Sn$_{0.125}$. Compared to In, Sn has one additional electron and acts as an electron donor in the substitution variant. For easy comparison, the DOS of the parent compound is also included in the figure.
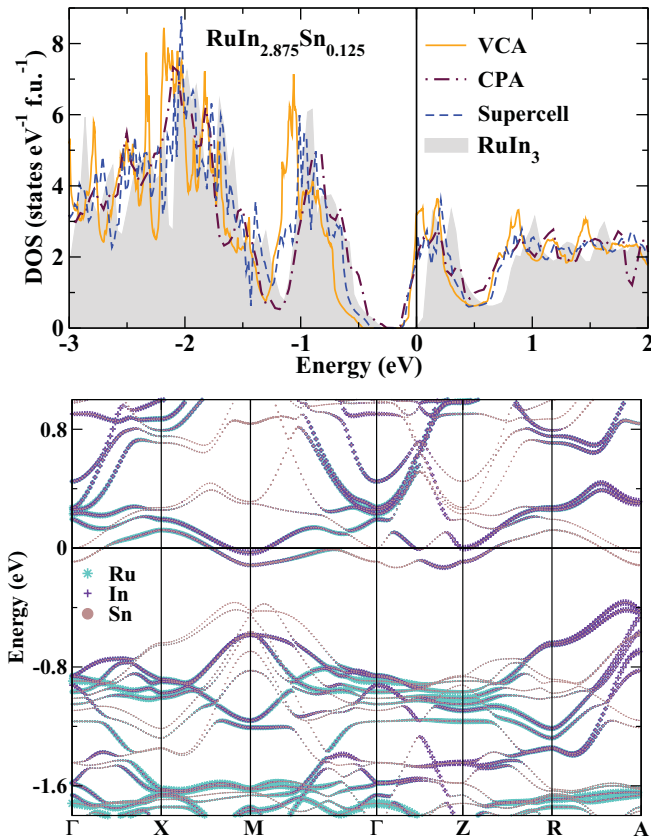

FIG. 3. (Color online) (Top panel) Calculated electronic DOS for the substitution derivative RuIn$_{2.875}$Sn$_{0.125}$ and the binary compound RuIn$_3$ as a reference. The vertical line at zero energy denotes the Fermi level and has been set to the bottom of the conduction band of the parent compound for easy visualization of the changes upon electron doping. The features close to the Fermi level are quite similar for the VCA, the CPA, and the SC approaches and change the DOS in a rigid-band-like fashion compared to the parent compound. The difference between the VCA and the SC approaches below −0.3 eV arises from the fact that within the SC approach the introduction of an actual Sn atom with a larger extent of the 5p orbitals increases the 4d-5p bandwidth. Disorder induced broadening is also observed for the CPA DOS. (Bottom panel) The nonmagnetic site projected band structure of RuIn$_{2.875}$Sn$_{0.125}$ using the SC approach. For easy comparison with the band structure of the binary compound in Fig. 2, the SC approach bands have been unfolded into the smaller tetragonal unit cell. The bands crossing the Fermi level have both In and Sn characteristics.

RuIn$_{2.875}$Sn$_{0.125}$ is metallic compared to the parent compound which is semiconducting (see Fig. 2). The shape of the DOS close to the Fermi edge is quite similar between the VCA, the CPA, and the SC approach for RuIn$_{2.875}$Sn$_{0.125}$. The slight dissimilarity in the DOS away from the Fermi edge arises from the underlying differences in the methodologies. Explicit inclusion (as compared to the VCA) of the Sn atom with the more extended 5p orbitals in the ordered SC approach results in a larger bandwidth of the Ru-4d–In-5p–Sn-5p hybridized states. This is clearly discernible in the DOS below −0.3 eV. Similarly, disorder induced incoherence of the valence band is also noticed for the CPA derived DOS below −0.3 eV. As mentioned previously, there are two crystallographically inequivalent indium positions in this structure (In1 at 4c and In2 at 8j). Hence, for each SC, two different calculations were performed by placing the substituent Sn once at the 4c position and once at the 8j position. The Sn atom preferentially occupies the 8j (In2) position, which is energetically favorable by 20 meV per formula unit compared to the 4c (In1) position. The bottom panel of Fig. 3 shows the nonmagnetic band structure of RuIn$_{2.875}$Sn$_{0.125}$ obtained using the SC approach. For a 4.2% substitution, the original unit cell of the binary compound has been doubled along the z axis, resulting in a smaller Brillouin zone (BZ). This has two consequences: first there are twice the number of bands, and second all the bands are folded back into the small BZ of the SC. The resulting band picture gets quite complicated, and it becomes hard to discern meaningful information from it. To facilitate easy comparison with the band structure of the binary compound, we have unfolded the bands according to the translational symmetry of the original unit cell using the approach described in Refs. [34] and [35]. The Ru and In characteristic unfolded bands of the SC in Fig. 3 are comparable to the bands in Fig. 2, though most of the degeneracies are lifted due to the presence of the Sn substituent. The size of the symbols in the band structure plot refers to the k-resolved weight of all the orbitals of the chosen site. The larger the size of the symbol, the larger is the contribution of the site to the band structure. Based on this, we can conclude that the bands crossing the Fermi level have both In and Sn characteristics, which is comprehensible due to the fact that Sn acts as an electron donor, making the system metallic, and is only one atomic number away from In in the periodic table, and hence similar to In.

Comparing the DOS of the binary RuIn$_3$ with that of RuIn$_{2.875}$Sn$_{0.125}$, we observe a rather rigid-band-like shift in the electronic structure. Similar behavior is observed for other substitution concentrations (not shown here). This result is extremely interesting from a technological point of view. Mahan and Sofo[2] showed that a narrow distribution of the energy of the electrons participating in the transport process is needed to maximize thermoelectric efficiency. The binary RuIn$_3$ possesses sharp peaklike features close to the conduction band minimum and as well as near the valence band maximum. Electron doping, as shown here using Sn as a substituent, results in a rigid-band shift of the DOS without adversely affecting the sharp peaklike features, thereby opening the possibility of fine tuning the substitution to achieve maximum thermoelectric efficiency. This will be discussed in detail in Sec. V.

C. $RuIn_{3-x}Zn_x$: hole doping

Following the same steps as described above for the Sn substitution, we have calculated the electronic structure of the Zn substituted system as well. Collected in Fig. 4 are the DOS and unfolded band structure for the 4.2% substitution scenario $RuIn_{2.875}Zn_{0.125}$. Substitution of Zn introduces holes into the system making $RuIn_{2.875}Zn_{0.125}$ metallic compared to the binary $RuIn_3$. Similar to the observations in the electron-doped system, the DOS close to the Fermi edge in the hole-doped variant is comparable between the VCA, the CPA, and the SC approaches. Moreover, the $3d$ orbitals of Zn are less extended and fully filled, resulting in strong In characteristics of the
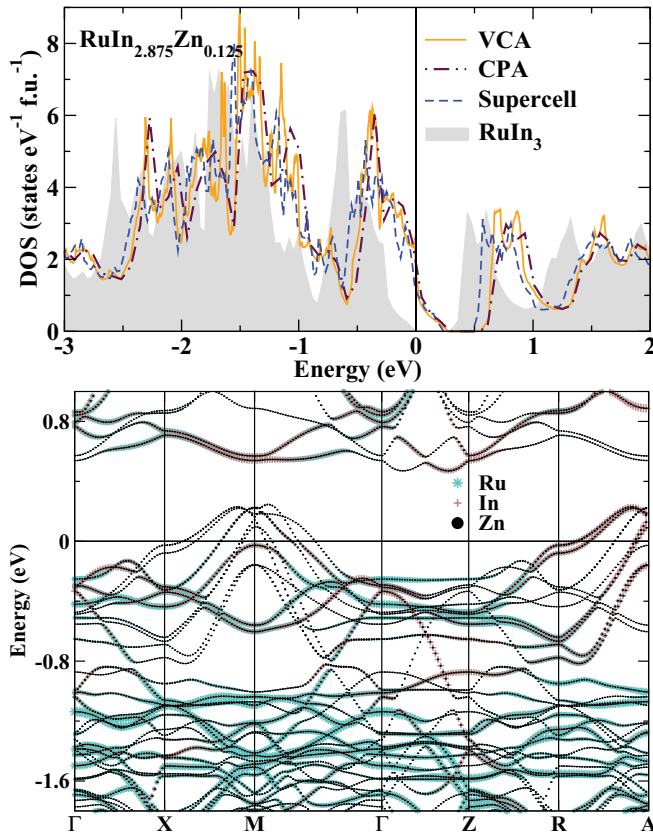

FIG. 4. (Color online) (Top panel) Calculated electronic DOS for the substitution derivative $RuIn_{2.875}Zn_{0.125}$ and the binary $RuIn_3$ for reference. The vertical line at zero energy denotes the Fermi level and has been set at the top of the valence band of the parent compound for easy visualization of the changes upon hole doping. The VCA, the CPA, and the SC approaches result in a metallic ground state with similar features of the DOS close to the Fermi edge. Analogous to the electron doping results, the changes in the DOS for the hole-doped system are again rigid-band-like. In contrast to Sn doping (see caption of Fig. 3), Zn $4d$ orbitals are not that extended, and hence the valence band spectrum is quite similar for both the VCA and the SC approaches. (Bottom panel) The nonmagnetic site projected band structure of $RuIn_{2.875}Zn_{0.125}$ using the SC approach. For easy comparison with the band structure of the parent compound in Fig. 2, the SC approach bands have been unfolded into the smaller tetragonal unit cell. The bands crossing the Fermi level have strong In characteristics.

bands that cross the Fermi level. Nevertheless, the changes in the DOS close to the Fermi level are still rigid-band-like, beneficial in tuning transport properties. Contrary to the Sn doping scenario, Zn atoms desirably occupy the $4c$ (In1) position which is energetically favorable by 27 meV per formula unit compared to the $8j$ (In2) position. This difference in preferred site occupations between the two substituents can be construed as follows: In2 atoms form a distorted trigonal prism with a Ru atom at its center (refer to Fig. 1). Extended p orbitals of the anions are necessary to facilitate the hybridization with the narrow d bands of the transition metal cations at the center of the distorted trigonal prism. Hence, Sn atoms which possess extended and partially filled p orbitals preferentially occupy the In2 position. Contrariwise, the transition metal Zn atom lacks extended p-like orbitals and hence preferentially occupies the In1 position, which is at the center of a distorted cube made of eight neighboring In2 atoms. Our theoretical observation of the preferential site occupation for the Zn atom is consistent with the experimental observation in another isotypic system $CoIn_{3-x}Zn_x$.[36] Using X-ray diffraction and neutron powder diffraction experiments, the authors observed that the substitution of In by Zn takes place in an ordered fashion, producing colored variants of the parent compound $CoIn_3$ with the Zn atom entering exclusively the position corresponding to the cube centers.

At this juncture, it should be noted that the proclivity of the substituent to certain indium sites is discerned only from the differences in the total energies of the various supercell configurations. No strongly distinguishable relevant features are noticeable in the DOS plots when Sn(Zn) occupies either In1 or In2 position and a similar rigid-band-like shift of the DOS compared to the binary $RuIn_3$ is noticed for all considered configurations. This observation is relevant for the experiments, where the fine tuning of the doped samples can be performed without the fear of adversely affecting the electronic structure of the final compound. Additionally, the metallic radii of In and Sn are similar (≈ 1.60 Å) and hence size effects do not play a significant role for the electron-doped systems. On the other hand, the metallic radius of Zn is about 13% smaller (≈ 1.40 Å) than that of In, and hence Zn is incorporated easily as a substitute for In in $RuIn_3$. Owing to the smaller metallic radius of the dopant Zn, there is a likelihood for a local structural relaxation around the dopant which could have a detrimental effect on the thermoelectric transport by altering the electronic properties of the host. We have investigated this in detail, by allowing for the local relaxation around the Zn atom in $RuIn_{3-x}Zn_x$ with $x = 0.125$. In the unrelaxed structure, the Zn atom (occupying the In1 position) is surrounded by a distorted cube of In2 atoms (see Fig. 1) with four In2 neighbors at 3.16 Å and another four In2 neighbors at 3.26 Å. The Ru-Zn bond length is 2.65 Å. The structural relaxation reduces the Zn-In2 bond length by just 2%, while the Ru-Zn bond length on the other hand is slightly increased to 2.70 Å. Nevertheless, these changes did not alter the electronic structure significantly, likely since the trigonal prisms centered around Ru and the cubes centered around the In1 site are heavily distorted, already in the undoped system.

V. THERMOELECTRIC PROPERTIES

A. Calculations

Having an improved understanding of the electronic properties of $RuIn_{3-x}A_x$ ($A =$ Sn, Zn) systems, we now calculate the transport coefficients using the semiclassical Boltzmann theory and the rigid-band approach. Such a procedure has been shown to successfully predict optimal doping levels in other thermoelectric materials, for example clathrates[29] and Sb_2Te_3.[37] One main concern when calculating transport coefficients is the underestimation of band gaps using the standard DFT functionals. Such an underestimation of band gaps manifests itself in the reduction of thermopower at higher temperatures due to bipolar conduction. To overcome this problem, we concentrate on analyzing the trend in the calculated thermopower for various concentrations of electron and hole doping rather than quantifying them. This approach results in a consistent scenario between experiment and theory as shown below. First, as seen in Fig. 2, it is important to note that the valence and conduction band of the stoichiometric compound are parabolic. As shown above, both Sn and Zn substitution act in a rigid-band-like fashion. Therefore, for small amounts of substituents, the bands will continue to remain parabolic. Hence, experimentally the transport can be modeled using simple parabolic band expressions to obtain the concentration of charge carriers in the system. We also notice that close to the conduction band minimum, there are multiple heavy bands (i.e., bands with less dispersion and hence larger effective mass), which is advantageous for thermoelectric transport. In contrast, the valence band maximum has a larger energy difference to the next available heavy band. Consequently, from just the viewpoint of electronic structure, an *n*-type material would retain better thermoelectric transport coefficients than a *p* type for low doping concentrations and low temperatures.

The values of the calculated thermopower are not affected by the constant scattering time approximation used to calculate the various transport properties, since the expression for S is independent of τ. This means that S is directly dependent on the electronic structure of the material. Collected in Fig. 5 is the temperature dependence of thermopower for various substitution concentrations of Zn and Sn in $RuIn_3$. Sn substitution introduces additional electrons into the system resulting in negative values of thermopower. Correspondingly, we obtain positive values of thermopower for Zn substitution which introduces holes in the system. Due to the lack of Hall data on all the measured samples, the assignment of the substitution concentration for the plots here are done by comparing the experimental thermopower measurements with the calculated values. For all substitution concentrations considered here, the magnitude of S increases steeply with temperature until 300 K. Above 300 K, in $RuIn_{3-x}Sn_x$, $|S|$ slightly reduces or remains constant. On the other hand, for $RuIn_{3-x}Zn_x$, $|S|$ above 300 K continues to increase with a smaller slope. Below room temperature and for $x \leqslant 0.050$, $|S|$ for the electron-doped system is 1.5 times that of the hole-doped system, consistent with the electronic band structure. In contrast, with increased doping ($x > 0.050$) and temperatures ($T > 300$ K), hole-doped $RuIn_{3-x}Zn_x$ shows increased thermopower compared to the electron-doped $RuIn_{3-x}Sn_x$. The
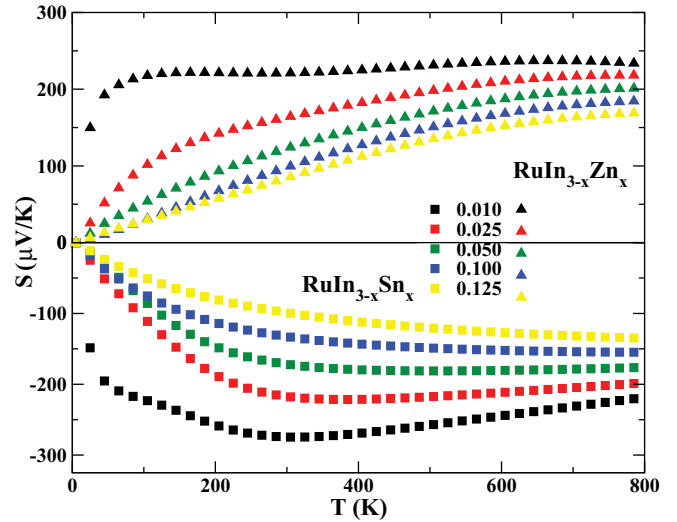
FIG. 5. (Color online) Thermopower S as a function of temperature for both Zn and Sn substitution variants $RuIn_{3-x}A_x$. A negative sign in S represents *n*-type behavior, and a positive sign in S represents *p*-type behavior. This figure is directly comparable to the experimental data from Ref. 15.

maximum values of $|S|$ (larger than 200 μV/K) are obtained for the smallest doping concentrations in both *p* and *n* types. Our results, including the absolute values of S, as well as the trend upon increased doping for the *n* type, are consistent with the recent experimental measurements.[15] A direct comparison of calculations for the *p* type with the recently published experiments is inhibited by the presence of impurity phase ZnO in the measured samples, and hence no clear trend is discernible from the experiments.[15] Presently, stimulated by our calculational results, we have successfully synthesized a new batch of ZnO free $RuIn_{3-x}Zn_x$ samples and measured their thermoelectric properties (details described in Sec. VI). The trend in measured S is now consistent with our calculated results for the *p*-doped systems too [refer to Fig. 10(a)].

Furthermore, transport measurements on the parent compound $RuIn_3$ find a change in the sign of S from *n* type to *p* type around 350 K. Similar behavior was observed for the related compound $RuGa_3$.[38] The authors assigned the sign change in S to the shift of the valence band to an extrinsic region along with the presence of light holes in the system and proposed a two-band model, one each for electron and hole, respectively, for evaluating S. In this scenario, holes with higher mobilities can influence S and change the sign from negative to positive values.[38] However, modeling transport properties including the presence of extrinsic charge carriers within a bulk system is more involved and beyond the scope of the present investigation.

As discussed earlier, notwithstanding the tetragonal symmetry of the crystal structure of $RuIn_3$, the polyhedra of the basic building blocks form a three-dimensional packing. Previously, measurements on single crystals of $RuIn_3$ have found a somewhat weak anisotropic resistivity along the [110] and [001] orientations.[14] Collected in Fig. 6 are the values of S and σ/τ along the crystallographic *a* and *c* directions. Consistent with the three-dimensional packing of polyhedra, the anisotropy is moderate in the calculated
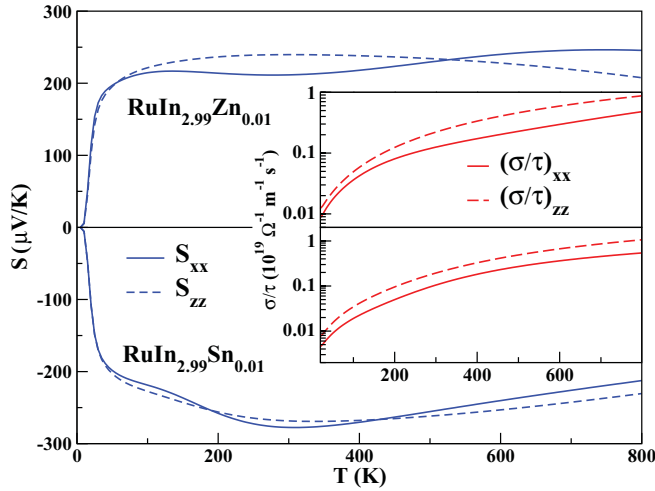
FIG. 6. (Color online) The main panel shows the calculated thermopower S and the inset shows the electrical conductivity σ relative to the relaxation time τ resolved along the crystallographic a [S_{xx}, $(\sigma/\tau)_{xx}$] and c [S_{zz}, $(\sigma/\tau)_{zz}$] directions.

FIG. 8. (Color online) Calculated power factor $S^2\sigma$ with respect to relaxation time τ as a function of temperature for both Zn and Sn substitution variants of RuIn$_{3-x}A_x$.

transport coefficients, with the p-doped system displaying a larger anisotropy than that of the n-doped variant. This result can be qualitatively understood by analyzing the band structures shown in Figs. 3 and 4. For the n-doped system, the bands crossing the Fermi level disperse in a similar fashion along the various symmetry directions. On the contrary, for the p-doped system, the bands crossing the Fermi level are more dispersive in the a-b plane ($X \Longrightarrow M \Longrightarrow \Gamma$) compared to the c direction ($\Gamma \Longrightarrow Z$).

Collected in Fig. 7 are the calculated electrical conductivities σ relative to the relaxation time τ for the same set of systems considered in Fig. 5. Note that σ has a linear dependence to τ. Assuming a constant τ for the various substitution variants, the increasing conductivity for either hole or electron doping reflects the fact that more charge carriers are present for the transport process. Due to the
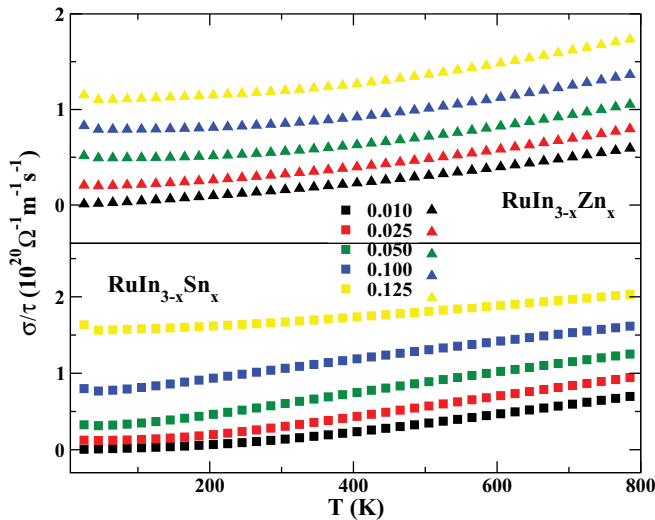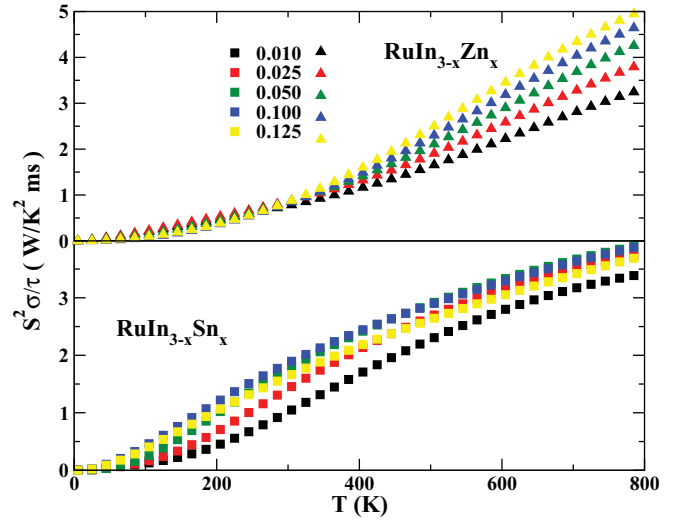
presence of a rather flat band with a larger effective mass close to the conduction band minimum, Sn substituted systems exhibit smaller electrical conductivities compared to the Zn substituted systems at low temperatures and low substitution concentrations. The trend observed for the thermopower previously is thus different than that of the conductivity, which will result in an interesting trend for the power factor $S^2\sigma$, the numerator in the expression for the thermoelectric figure of merit zT. To this end, we have plotted $S^2\sigma$ relative to the relaxation time τ in Fig. 8. For temperatures up to 300 K, the power factors of the Sn substituted systems are enhanced compared to those of the Zn substituted systems. Beyond 300 K, the trend is reversed and the hole-doped systems exhibit an enhanced power factor. A quantitative estimate for the dimensionless figure of merit zT from DFT entails an accurate estimation of κ_{ph}, the lattice thermal conductivity. This involves solving the phonon Boltzmann transport equations exactly and requires an accurate description of the harmonic and anharmonic interatomic forces, which is presently a formidable task and is left for a more extended study in the future. Additionally, disorder and nanostructuring effects that arise during experiments modify κ_{ph} in a not so straightforward way for a concise theoretical description. Nevertheless, clues provided by the transport coefficients that are directly dependent on the electronic structure have been used to successfully tune the thermoelectric properties of other known materials.[29,36,37] In the case of RuIn$_{3-x}$Sn$_x$ and RuIn$_{3-x}$Zn$_x$, our calculations of the power factor establish a robust scenario for both p- and n-doped systems with improved values for certain doping levels.

B. Experimental data for RuIn$_{3-x}$Zn$_x$

The chemical analysis of the commercially available starting materials (Ru, In, and Zn) showed a measurable amount of oxygen content only in the case of Ru: 0.54 mass % of oxygen, which is presumably present in the form of RuO$_2$. This oxide impurity is completely removed via hydrogen reduction at
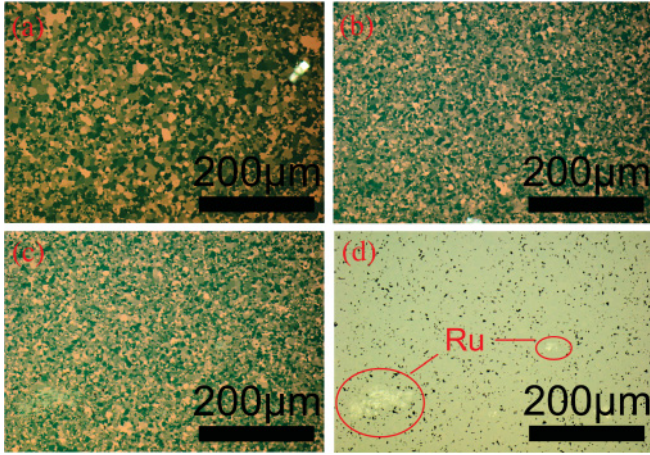

FIG. 7. (Color online) Calculated electrical conductivities σ relative to relaxation time τ as a function of temperature for both Zn and Sn substitution variants of RuIn$_{3-x}A_x$.

FIG. 9. (Color online) Microstructure of $RuIn_{3-x}Zn_x$ samples: (a) $x = 0.025$, polarized light; (b) $x = 0.050$, polarized light, the surface is perpendicular to the pressure direction during the SPS treatment; (c) $x = 0.050$, polarized light, the surface is parallel to the pressure direction during the SPS treatment; and (d) $x = 0.050$, bright light.

900 °C for 5 h in a home-made setup (O_2 not detectable after H_2 reduction). After this hydrogen treatment, the samples were prepared strictly in accord with the description in Ref. 15. Microstructure analysis of $RuIn_{2.975}Zn_{0.025}$ [Fig. 9(a)] shows single-phase homogenous products without any ZnO impurity. Only in the case of $RuIn_{2.95}Zn_{0.05}$ and $RuIn_{2.90}Zn_{0.10}$, small trace amounts of residual Ru were found [Fig. 9(d)], which might be due to the defect occupation of the Ru site. The grains, with respect to their size, shape, and orientation are quite similar for all the samples discussed here. Additionally, the microstructure is independent from the substitution concentration of Zn, and the direction of pressure during the spark plasma sintering (SPS) experiments [Figs. 9(b) and 9(c)]. The X-ray diffraction patterns of the $RuIn_{3-x}Zn_x$ samples were indexed with the $P4_2/mnm$ (No. 136) space group. Compared to the previously published results,[15] the a lattice parameter remains unchanged, while the c lattice parameter is slightly reduced (Table I). For the composition of the samples, see Ref. 39. Because of the absence of ZnO impurities, all of the Zn has been incorporated into the lattice, resulting in a pronounced reduction of the unit cell in the c direction.

The transport-related quantities and the resultant figure of merit zT are collected in Fig. 10. The temperature dependence of the electrical resistivity ρ shows metallic behavior for all the substitution derivatives, with increasing resistivity for increasing temperature. The absolute values of ρ shown here are reduced in comparison to our previously published results[15] due to the absence of the ZnO impurity phase, which is an insulator with a large band gap of more than 3 eV.

TABLE I. Refined lattice parameters for $RuIn_{3-x}Zn_x$

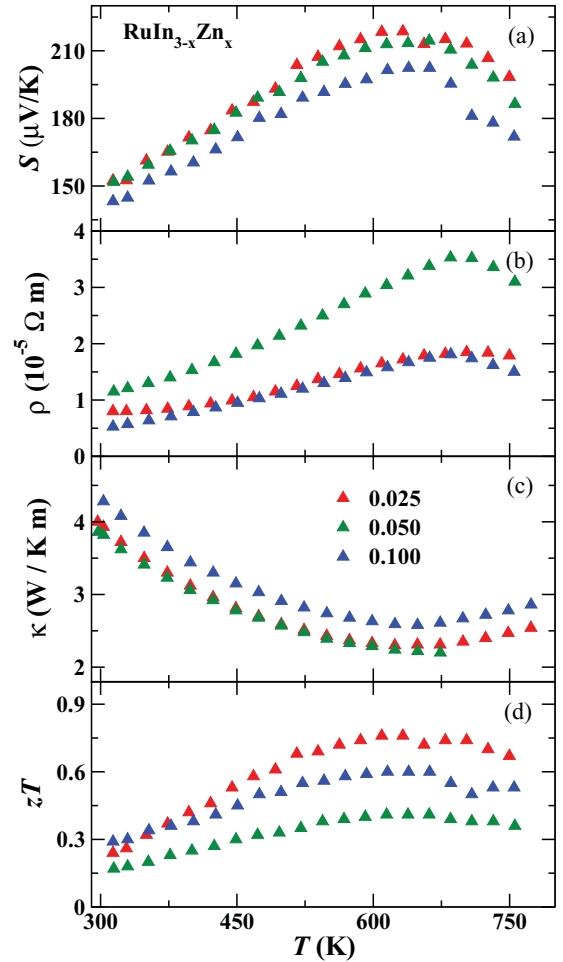| x	a (Å)	c (Å)
0.025	6.9988(1)	7.2456(2)
0.050	6.9988(1)	7.2396(1)
0.100	6.9977(2)	7.2422(3)

FIG. 10. (Color online) Measured thermoelectric properties of $RuIn_{3-x}Zn_x$ as a function of temperature. (a) Seebeck coefficient S, (b) electrical resistivity ρ, (c) total thermal conductivity κ, and (d) dimensional figure of merit zT.

The measured thermopower S is positive (p type) and is reducing with increasing x. At 350 K, the absolute values of S_{exp} change from 162 to 150 μV/K for $0.025 \leqslant x \leqslant 0.100$, compared to our calculations where S_{theo} change from 170 to 115 μV/K. For all the samples considered here, S increases with increasing temperature and reaches a maximum around 600 K. This trend in S as a function of x and the temperature are now consistent with our above mentioned theoretical predictions (Fig. 5). The thermal conductivity κ is only slightly increased in comparison to Ref. 15. Previously, the presence of ZnO impurities could have acted as additional scatterers to reduce κ, which is presently removed from our samples. The temperature dependence of the dimensionless figure of merit zT increases strongly, reaching a value of 0.8 at 620 K for $RuIn_{2.975}Zn_{0.025}$. Albeit the trend in S is congruent between experiment and theory, the same cannot be inferred for the other transport related quantities and hence zT, because of the complex dependency relations between these parameters. While the expression for S is free of parameters, ρ, κ, and hence zT are dependent on the scattering time τ. Our calculations which are based on the constant scattering time approximation cannot be expected to yield more realistic

results. Nonetheless, we have demonstrated that insights from band structure calculations can be quite helpful in fine tuning thermoelectric properties.

VI. CONCLUSIONS

We have analyzed in detail the electronic structure of the hole- and electron-doped $RuIn_3$ intermetallic compound. We have used various methods to model the effects of doping, starting from the simple VCA description to the time consuming and the more reliable CPA approach. Effects of ordering of the dopant were also considered using the SC approach. Comparing the results of the VCA, the CPA, and the SC approach, we can conclusively determine that the dopants introduce charge carriers and change the electronic structure in a rigid-band-like fashion. This scenario allows for the advantageous use of the sharp peaklike features in the DOS to obtain good thermoelectric properties. Transport coefficients (thermopower and power factor) calculated using the semiclassical Boltzmann transport equations are in good agreement with the experimental results. Based on our calculations, we can conclude that low substitution levels are advantageous in obtaining large values of thermopower. Both n- and p-doped systems have similar transport properties. In particular, based on our calculations, for $T \geqslant 400$ K, p-doped samples with $x \geqslant 0.125$ show considerable potential for improving the figure of merit zT. Similarly, for $T \leqslant 500$ K,

n-doped systems with an optimal substitution in the range $0.050 \leqslant x \leqslant 0.100$ also show great thermoelectric potential. A $zT \approx 0.8$ has been obtained for $RuIn_{2.975}Zn_{0.025}$, while the first trial of experiments were able to only reach a $zT \approx 0.1$ in the n-doped samples.[15] Additional experimental investigations exploring higher p-dopant concentrations as well as fine tuning the n-doped systems are desirable to probe the possibility of further enhancing zT. $RuIn_{3-x}A_x$ ($A =$ Sn, Zn) systems with their robust electronic properties, containing a low-toxic combination of elements, provide— although expensive—an ideal playground for experimentalists to investigate in detail and tune the thermoelectric properties as a function of doping. Our combined results of theoretical calculations and experimental work has clearly demonstrated that narrow-band-gap semiconductors formed by transition-metal atoms with groups III, IV, and V elements have a large potential in thermoelectric applications. The presented study will, hopefully, also stimulate the search for new better and cheaper systems in this family of compounds whose properties follow the same underlying physics as $RuIn_{3-x}A_x$ ($A =$ Sn, Zn).

[1]G. Aeppli and Z. Fisk, Comments Condens. Matter Phys. **16**, 155 (1992).

[2]G. D. Mahan and J. O. Sofo, Proc. Natl. Acad. Sci. USA **93**, 7436 (1996).

[3]V. Jaccarina, G. K. Wertheim, J. H. Wernick, L. R. Walker, and S. Arajs, Phys. Rev. **160**, 476 (1967).

[4]A. Bentien, S. Johnsen, G. K. H. Madsen, B. B. Iversen, and F. Steglich, Europhys. Lett. **80**, 17008 (2007).

[5]N. Tsujii, H. Yamaoka, M. Matsunami, R. Eguchi, Y. Ishida, Y. Senba, H. Ohashi, S. Shin, T. Furubayashi, H. Abe, and H. Kitazawa, J. Phys. Soc. Jpn. **77**, 024705 (2008).

[6]P. S. Riseborough, Adv. Phys. **49**, 257 (2000).

[7]J. K. Freericks, D. O. Demchenko, A. V. Joura, and V. Zlatić, Phys. Rev. B **68**, 195120 (2003).

[8]B. C. Sales, E. C. Jones, B. C. Chakoumakos, J. A. Fernandez-Baca, H. E. Harmon, J. W. Sharp, and E. H. Volckmann, Phys. Rev. B **50**, 8207 (1994).

[9]Y. Hadano, S. Narazu, M. A. Avila, T. Onimaru, and T. Takabatake, J. Phys. Soc. Jpn. **78**, 013702 (2009).

[10]K. Schubert, H. L. Likas, H. Meissner, and S. Bhan, Z. Metallkd. **50**, 534 (1959).

[11]H. Holleck, H. Nowotny, and F. Benesovsky, Monatsh. Chem. **95**, 1386 (1964).

[12]R. Pöttgen, J. Alloys Compd. **226**, 59 (1995).

[13]U. Häussermann, M. Bottröm, P. Viklund, Ö. Rapp, and T. Björnängen, J. Solid State Chem. **165**, 94 (2002).

[14]D. Bogdanov, K. Winzer, I. A. Nekrasov, and T. Pruschke, J. Phys. Condens. Matter **19**, 232202 (2007).

[15]M. Wagner, R. Cardoso-Gil, N. Oeschler, H. Rosner, and Yu. Grin, J. Mater. Res. **26**, 1886 (2011).

[16]Y. Imai and A. Watanabe, Intermetallics **14**, 722 (2006).

[17]A. Mani, S. Sharma, S. Chandra, and A. Bharathi, J. Phys. Condens. Matter **23**, 205802 (2011).

[18]R. P. Mertens, R. J. Van Overstraeten, and H. J. DeMan, in *Advances in Electronics and Electron Physics*, edited by L. Marton and C. Marton (Academic, New York, 1981), Vol. 55, pp. 77–118.

[19]K. Koepernik and H. Eschrig, Phys. Rev. B **59**, 1743 (1999).

[20]I. Opahle, K. Koepernik, and H. Eschrig, Phys. Rev. B **60**, 14035 (1999).

[21]J. P. Perdew and Y. Wang, Phys. Rev. B **45**, 13244 (1992).

[22]Calculations using the generalized gradient approximation (GGA) yield a very similar physical picture and confirm the robustness of our results.

[23]The lattice parameter for $x = 0.125$ is obtained by extrapolating linearly the experimental data from Ref. 15.

[24]K. Koepernik, B. Velick, R. Hayn, and H. Eschrig, Phys. Rev. B **55**, 5717 (1997).

[25]D. Kasinathan, A. Ormeci, K. Koch, U. Burkhardt, W. Schnelle, A. Leithe-Jasper, and H. Rosner, New J. Phys. **11**, 025023 (2009).

[26]M. Schmitt, J. Málek, S.-L. Drechsler, and H. Rosner, Phys. Rev. B **80**, 205111 (2009).

[27]J. M. Ziman, *Electrons and Phonons* (Oxford University Press, New York, 2001).

[28]W. Jones and N. H. March, *Theoretical Solid State Physics* (Courier Dover, New York, 1985).

[29]G. K. H. Madsen, K. Schwarz, P. Blaha, and D. J. Singh, Phys. Rev. B **68**, 125212 (2003).

[30]G. K. H. Madsen and D. J. Singh, Comput. Phys. Commun. **175**, 67 (2006).

[31]S. Johnsen, A. Bentien, G. K. H. Madsen, Bo B. Iversen, and M. Nygren, Chem. Mater. **18**, 4633 (2006).

[32]D. J. Singh and D. Kasinathan, J. Electron. Mater. **36**, 736 (2007).

[33]H. J. Xiang and D. J. Singh, Phys. Rev. B **76**, 195111 (2007).

[34]W. Ku, T. Berlijn, and C.-C. Lee, Phys. Rev. Lett. **104**, 216401 (2010).

[35]E. van Heumen, J. Vuorinen, K. Koepernik, F. Massee, Y. Huang, M. Shi, J. Klei, J. Goedkoop, M. Lindroos, J. van den Brink, and M. S. Golden, Phys. Rev. Lett. **106**, 027002 (2011).

[36]P. Viklund, S. Lidin, P. Berastegui, and U. Haäussermann, J. Solid State Chem. **164**, 100 (2002).

[37]T. Thonhauser, T. J. Scheidemantel, J. O. Sofo, J. V. Badding, and G. D. Mahan, Phys. Rev. B **68**, 085201 (2003).

[38]Y. Amagai, A. Yamamoto, T. Iida, and Y. Takanashi, J. Appl. Phys. **96**, 5644 (2004).

[39]The experimental chemical composition obtained from energy- and wavelength-dispersive X-ray spectroscopy for nominal $RuIn_{2.975}Zn_{0.025}$ is $Ru_{0.91(3)}In_{2.96(2)}Zn_{0.04(2)}$ (from EDXS), for nominal $RuIn_{2.95}Zn_{0.05}$ is $Ru_{0.978(5)}In_{2.95(1)}Zn_{0.05(1)}$ (from WDXS), and for nominal $RuIn_{2.90}Zn_{0.1}$ is $Ru_{0.96(2)}In_{2.91(3)}Zn_{0.09(2)}$ (from EDXS).